14.4 INFRARED HYPERSPECTRAL SOUNDING MODELING AND PROCESSING: AN OVERVIEW

Hung-Lung Huang*, Chris Velden, Jun Li, Elisabeth Weisz, Kevin Baggett, James E. Davies, John Mecikalski, Bormin Huang, Russ Dengel, Steven A. Ackerman, Erik R. Olson, Robert O. Knuteson, Dave Tobin, Leslie Moy, Jason A. Otkin, Derek J. Posselt[%], Hank E. Revercomb, and William L. Smith[+]

Cooperative Institute for Meteorological Satellite Studies (CIMSS)
University of Wisconsin-Madison
[+]Langley Research Center, NASA
[%]Colorado State University, Department of Atmospheric Sciences

1. INTRODUCTION

Infrared hyperspectral sounding instruments with broad spectral coverage have the potential to provide unprecedented atmospheric profiling, surface characterization, cloud property and trace gas information. These instruments will be deployed on satellites in both polar orbit (for global coverage) and in geostationary orbit (for regional high temporal resolution coverage). Making best use of the improved measurement capabilities of, and the investment in, instruments such as CrIS, GIFTS, and HES demands efficient modeling and processing algorithms capable of generating data products for weather forecasting and other time critical applications with minimal time latency. This paper reviews the complete measurement and processing cycle from NWP modeling of the atmosphere, through the simulation of radiances emergent at the top of the atmosphere and finally to the processing of those radiances to retrieve atmospheric clear and cloudy sounding profiles.

Demonstration of GIFTS (Smith et al., 2000) and HES modeling and processing systems will illustrate the trend of future infrared sounding from space and its impact on the future strategy for global earth observation.

2. GIFTS CLEAR-SKY FORWARD MODELING

The GIFTS forward model is developed under the framework of Pressure Layer Optical Depth (PLOD). The clear sky fast model used at UW-CIMSS applies a PLOD regression (Hannon et al., 1996) to line-by-line calculations obtained with LBLRTM (Clough and Iacono, 1995) and the HITRAN '96 (Rothman et al., 1992) database. The line-by-line transmittance data were mapped to the GIFTS spectral domain using a maximum optical path difference of 0.872448 cm, with an effective spectral resolution of 0.6 cm^{-1}, and apodized (Mlawer et al., 2003) prior to performing the regression analysis.

Corresponding author address: Hung-Lung Allen Huang, Cooperative Institute for Meteorological Satellite Studies, University of Wisconsin-Madison, 1225 West Dayton Street, Madison, WI 53706; E-mail: allenh@ssec.wisc.edu

The key features of the UW-CIMSS GIFTS clear sky forward model can be summarized as follows:

1. LBLRTM v6.01 runs:
- HITRAN '96 + JPL extended spectral line parameters
- MTCKD5 v1.0 H_2O and 15 µm CO_2 continuum

2. Spectral Characteristics:
- ~586–2347 cm^{-1}
- ~0.8724 cm MOPD
- Kaiser Bessel #6 apodization

3. Fast Model:
- 32 profiles from NOAA database
- 6 view angles
- 100 vertical layers (equivalent to those used for AIRS)
- Three transmittance components: fixed gases, H_2O, and O_3
- AIRS PLOD predictors

4. Run time:
~0.8 sec on a 1 GHz CPU

Figure 1 displays the current planned spectral coverage of GIFTS measurements with clear-sky brightness temperature calculated from the U.S. standard atmosphere.

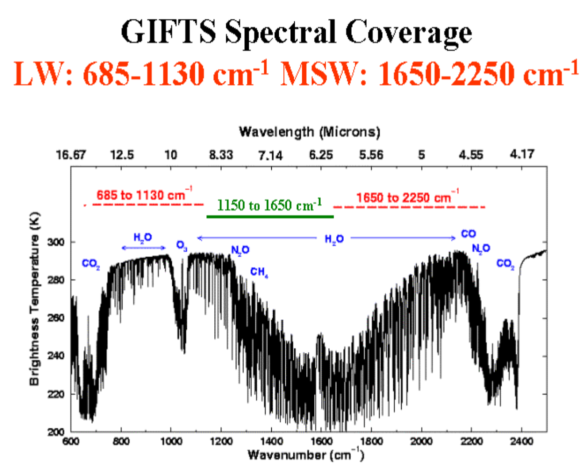

Fig. 1: GIFTS spectral coverage and the brightness temperature spectrum of a cloud-free atmosphere.

3. HYPERSPECTRAL CLOUD MODELING AND CLOUDY RADIANCE CALCULATION

Previous work on the GIFTS forward model's cloud component is summarized in Huang et al. (2000). Subsequent to that paper, a computer code to generate the bulk optical properties of water clouds has been developed. This code can be used to generate the optical thickness, single-scattering albedo, and asymmetry factor of the phase function for spectral regions 685–1130 and 1650–2250 cm^{-1} for a given effective droplet size, liquid water content (LWC), and cloud physical thickness. This research development consisted of two parts. In the first, extensive numerical computations were performed for the single-scattering properties of individual water droplets over the spectral ranges of interest (listed above). These properties were then applied to droplet size distributions with various effective sizes with the results tabulated as a large lookup table. The second part involved the development of an efficient two-dimensional interpolation scheme to generate the bulk optical properties of clouds at any wavenumber within the two spectral regions on the basis of the pre-calculated lookup table.

For scattering calculations of ice clouds at infrared wavelengths, there is no single method that can cover the range of practical particle sizes. For this reason, the finite-difference time domain method (FDTD) (Yang and Liou, 1996) was used for ice crystals smaller than 40 µm to calculate single-scattering properties of extinction efficiency, single-scattering albedo, and phase function. For larger particles, the newly developed stretched scattering potential method (SSPM) (Yang et al., 2001) was used to calculate the extinction and absorption efficiencies. Furthermore, the improved geometry optical method was used to derive the phase function. In atmospheric radiative transfer calculations, the phase function can be approximated by the well-known Henyey-Greenstein phase function based on the asymmetry factor.

Figure 2 shows the fast parameterized cloud optical thickness, single-scattering albedo, and emissivity for both water and ice clouds at various effective radii. Water clouds with particles larger than 15 microns exhibit spectral emissivities having very little spectral variation while those with smaller water cloud particles exhibit larger spectral emissivity variation. In contrast, ice clouds display a large variation in spectral emissivity for particles smaller than 50 microns.

Cloud transmittance is defined as the complement of cloud emissivity. Above the cloud level, the total transmittance profile is set equal to the clear component transmittance. Below the cloud level, total transmittance becomes the product of the cloud and clear component transmittance.

Radiances in the presence of clouds are simulated as the sum of four components that together account for both clear and cloudy atmospheric paths (Figure 3).

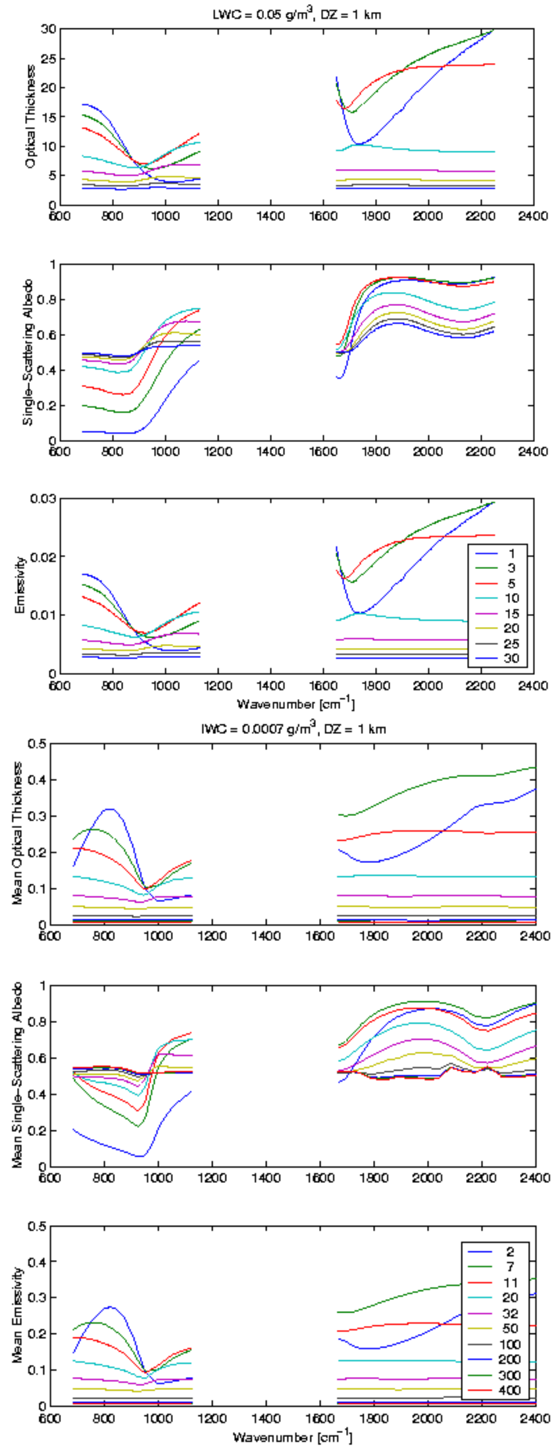

Fig. 2: Fast parameterized optical thickness, single-scattering albedo, and emissivity for water (upper panel) and ice (lower panel) clouds. Water clouds are assumed to be 1 km thick with a liquid water content of 0.005 g/m^3 and effective radii of 1, 3, 5, 10, 15, 20, 25 and 30 microns. Ice clouds are assumed to be 1 km thick with ice water content of 0.0007 g/m^3 and effective radii of 2, 7, 11, 20, 32, 50, 100, 200, 300 and 400 microns.

$$\tilde{I}_{top}(\mu) = I_0 T(\mu)\mathrm{T}_{a1}(\mu) + I_{cld}\mathrm{T}_{a1}(\mu) + I_1 + I_1^{\downarrow}\alpha(\mu)\mathrm{T}_{a1}(\mu)$$

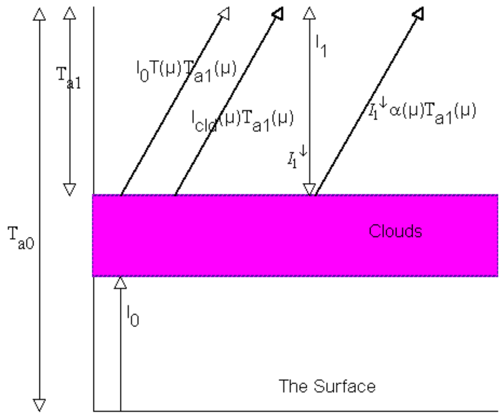

Where:

$$I_0 = B(t_s)\mathrm{T}_{a0} + \int_{\mathrm{T}_{a0}}^{\mathrm{T}_{a1}} B(t)d\mathrm{T}_a$$

$$I_1 = \int_{\mathrm{T}_{a1}}^{1} B(t)d\mathrm{T}_a$$

$$I_{cld}(\mu) = [1 - R(\mu) - T(\mu)] * B(t_c)$$

$$I_1^{\downarrow} = \int_{\mathrm{T}_{a1}}^{1} B(t)\frac{\mathrm{T}_{a1}}{\mathrm{T}_a^2}d\mathrm{T}_a$$

T_{a0} and T_{a1} are clear sky atmospheric transmission from the out space to the surface and to cloud top, respectively.

Fig. 3: Fast cloudy radiative transfer equation for parameterization of clouds (Yang, 2003).

Figure 4. shows three spectra simulated by this fast model. Fast outputs are compared to those predicted by LBLDIS (Turner 2003), a radiative transfer code which couples DISORT (Stamnes et al., 1988) with LBLRTM. For verification purposes the outputs of LBLDIS are considered "truth".

Comparisons are made for liquid and ice clouds, for a range of effective diameters, optical depths and cloud top altitudes. Figure 5 shows the RMS difference between fast model and "truth" brightness temperatures for the case of liquid cloud with a cloud top altitude of 2 km. Figure 6 shows the RMS differences for the case of ice cloud with a cloud top altitude of 10 km.

The effects of the cloud crystal habit, or particle shape, on the measured top of the atmosphere radiances in the infrared short to longwave regions are also under study. Figure 7 displays a preliminary result of this work. Clouds are located at 10 km height with a visible cloud optical thickness equal to 1 and effective ice crystal habits of sphere, hexagonal column, aggregates, bullet-rosette, and plate. The brightness temperature calculated at 8.55 µm shows significant differences for the different particle sizes and shapes.

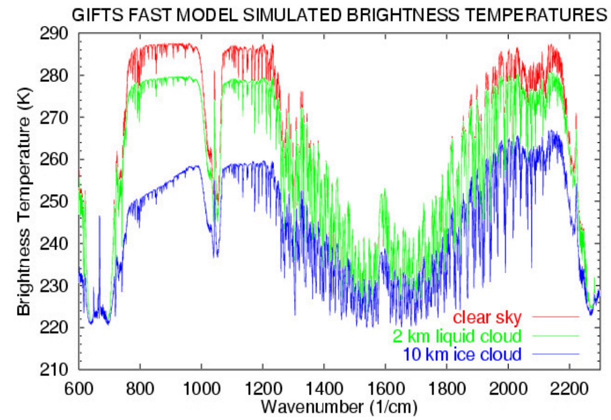

Fig. 4: Fast model simulated spectra at GIFTS spectral resolution for clear sky, liquid cloud at 2 km altitude and ice cloud at 10 km altitude. The ice cloud is comprised of hexagonal ice crystals and the liquid cloud is spherical droplets. In both cases the effective particle size is 40 µm and the optical depth is 2.

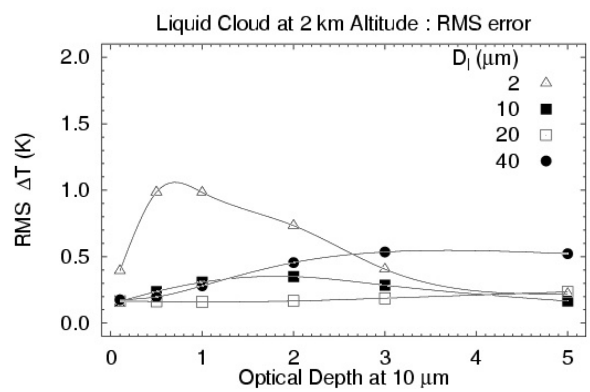

Fig 5: RMS difference between fast model and "truth" brightness temperatures for the case of liquid cloud with a cloud top altitude of 2 km.

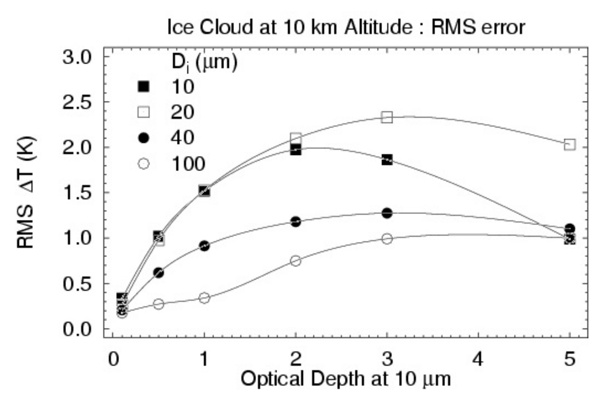

Fig 6: RMS difference between fast model and "truth" brightness temperatures for the case of ice cloud with a cloud top altitude of 10 km.

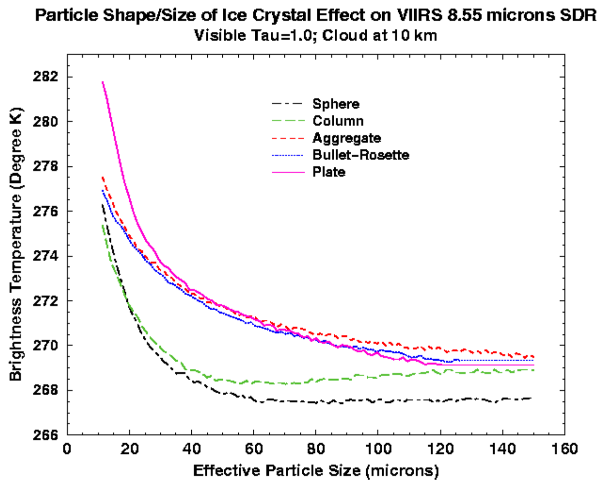

Fig. 7: Cloud particle shape effects on the 8.55 µm brightness temperature measurements as a function of effective particle sizes.

4. HYPERSPECTRAL MEASUREMENTS SIMULATION AND SOUNDING PROCESSING

The MM5 (Grell et al., 1994) mesoscale model has been used to simulate hyperspectral measurements. Some features of this model include:

- Arbitrary resolution in all directions
- Choice of Lambert Conformal, Mercator, or Polar Stereographic coordinate system in the horizontal
- Terrain-following sigma-p coordinate system
- Multiple two-way interactive grid nesting, with moveable inner grids
- Gridscale microphysics parameterization with cloud water, rain, ice, snow, and graupel
- Choice of several advanced cumulus parameterization schemes including Grell and Kain-Fritsch
- Long and Shortwave radiation parameterization with cloud effects. The longwave scheme is based on the AER RRTM radiative transfer code.
- Choice of boundary layer parameterization, including schemes with TKE prediction

The MM5 simulated mesoscale temporal atmospheric states and their corresponding top of the atmosphere calculated radiances have been used as a control data set for a variety of GIFTS trade studies and product algorithm development tasks. For example, an animation has been created that demonstrates the projected ability of GIFTS to remotely sense the environmental factors leading to the onset of convection. Figure 8 shows four time steps from the animation (during the IHOP experiment, from 1500 UTC of 12 June to 0000 UTC of 13 June, 2003) of the vertical water vapor distribution and wind vectors at an altitude of 1.8 km above sea level. The view is of the IHOP domain over Oklahoma and Kansas from a southern elevation. The front range of the Rocky Mountains can be seen on the underlying topographic map on the left-hand side. The horizontal extent of the domain depicted is 1000 × 1500 km; roughly equivalent to 2 × 3 GIFTS cubes as the resolution of this particular test simulation is 10 km in the horizontal while GIFTS will have 4 km resolution. White/gray clouds are evident for all the four time steps in northeast corner. The presentation will show the full resolution animation of the water vapor transport and cloud formulation.

Another MM5 simulation was produced for the last few days of the 2003 Pacific THORPEX experiment. This simulation used a Lambert Conformal projection with 3 two-way interactive nested domains. The physical parameterizations included the Eta planetary boundary layer scheme, explicit convection on the innermost domain with the Grell cumulus scheme used on the outer two domains, Goddard microphysics, and RRTM/Dudhia radiation scheme.

The meteorological situation for this simulation shows an intense zonally-oriented jet stream with winds over 90 m/s at 300 hPa that was present across the north-central Pacific Ocean. On the anticyclonic side of this jet stream, relatively benign weather prevailed over the region corresponding to the southern half of the simulated domain. However, to the north of this jet stream, a series of disturbances were progressing across the Pacific. A well-defined circulation in the cloud fields across the northern portion of the simulated domain was associated with a rather strong occluded cyclone, resulting in a region of scattered showers and squalls to the southeast of this cyclone's center. Very brisk winds were present at the surface across much of the domain with surface winds in excess of 20 m/s across the middle of the domain. Near the end of the simulation, a cirrus cloud band associated with a plume of tropical moisture ahead of an advancing cyclone to the west of the simulation domain was beginning to advect into the domain.

The MM5 model was also used to generate a model atmosphere for input to the forward model to simulate top of the atmosphere GIFTS radiances every half hour for the horizontal THORPEX domain of 1500 by 1500 km. Figure 9 shows the 1-km altitude water vapor mixing ratio and clouds between 2100 UTC on March 12 2003, and 1200 UTC on March 13 2003. The relatively small spatial scale of the mixing ratio maxima/minima, especially along the northern half of the domain, indicates the ability of the MM5 model to simulate fine scale moisture fields and by, extension cloud fields. Along the southern half of the domain, the larger scale of the individual components of the mixing ratio field corresponds to a much more uniform low-level stratus cloud deck in this region.

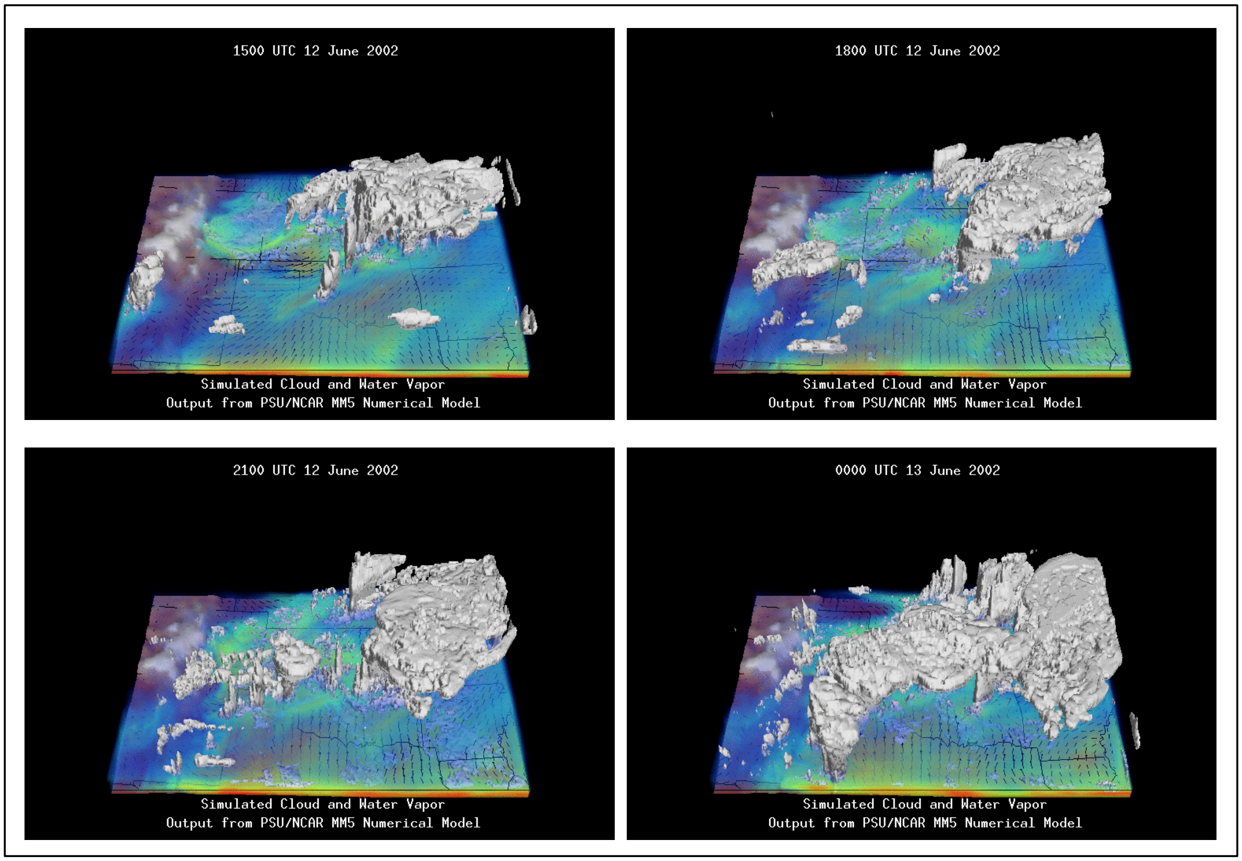

Fig. 8: Water vapor, wind and cloud fields derived from a 10 km horizontal resolution MM5 simulation of a convective initiation event that occurred on 12/13 June 2002 during the IHOP 2002 field campaign. UTC times shown are for 15:00 (top left), 18:00 (top right) and 21:00 (bottom left) of June 12, and 00:00 (bottom right) of June 13, 2003. The volume (haze) represents water vapor mixing ratio (g/kg), shaded from blue (lower mixing ratios) to red (high mixing ratios). Three-dimensional wind vectors are spaced every 50 km and are plotted at 1.8 km above sea level. White isosurfaces show the outer extent of modeled clouds including ice and water clouds.

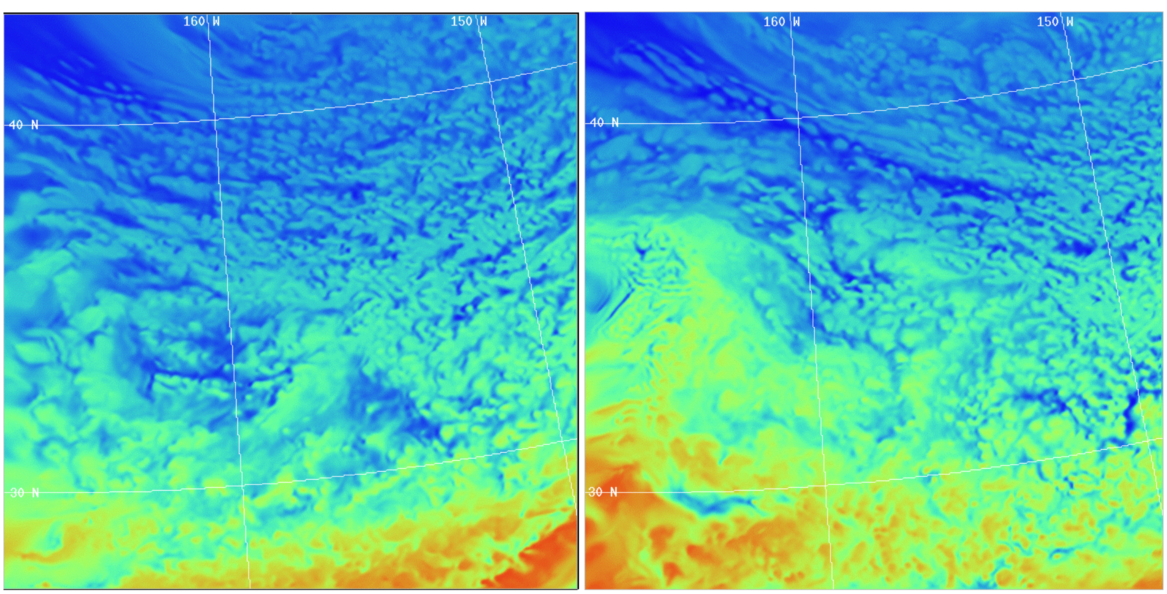

Fig. 9: Water vapor mixing ratio derived from MM5 at 2100UTC (left panel) on 12 March 2003, and 1200 UTC (right panel) on 13 March 2003. It is a colored horizontal figure at 1.0 km that clearly illustrates the abundance of low level moisture in the oceanic boundary layer.

Figure 10 shows the simplified GIFTS NOAA/NASA validation, concept demonstration and data processing flow diagram. The end-to-end level 0 to level 3 processing procedure demonstrates geosynchronous hyperspectral sounding profile and wind capability.

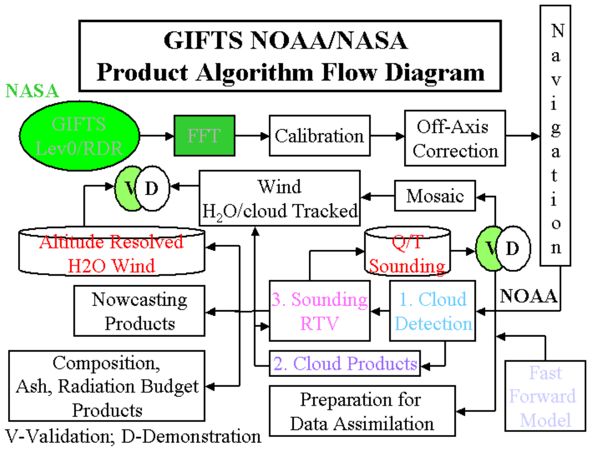

Fig. 10: GIFTS level 0 to level 3 data processing and product generation, validation, and demonstration flow diagram.

Figures 11 and 12 are examples of GIFTS retrieval demonstration using real Aqua AIRS and IHOP simulated hyperspectral radiances. Currently, GIFTS will only perform retrieval under clear-sky conditions. The cloudy sounding retrieval algorithm is under development and will be reported on when those results become available.

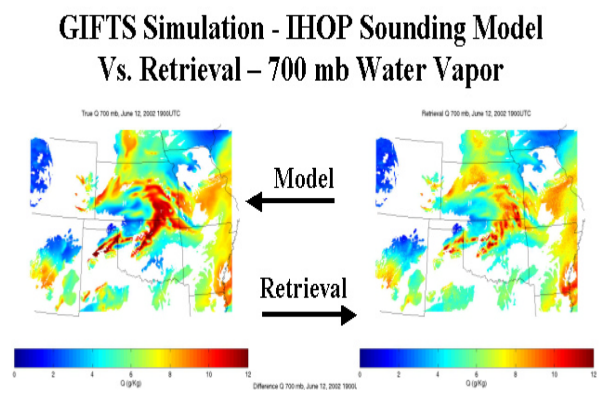

Fig. 12: Simulated IHOP GIFTS clear-sky water vapor retrieval demonstration. GIFTS water vapor (right panel) is compared with MM5 model "truth" (left panel).

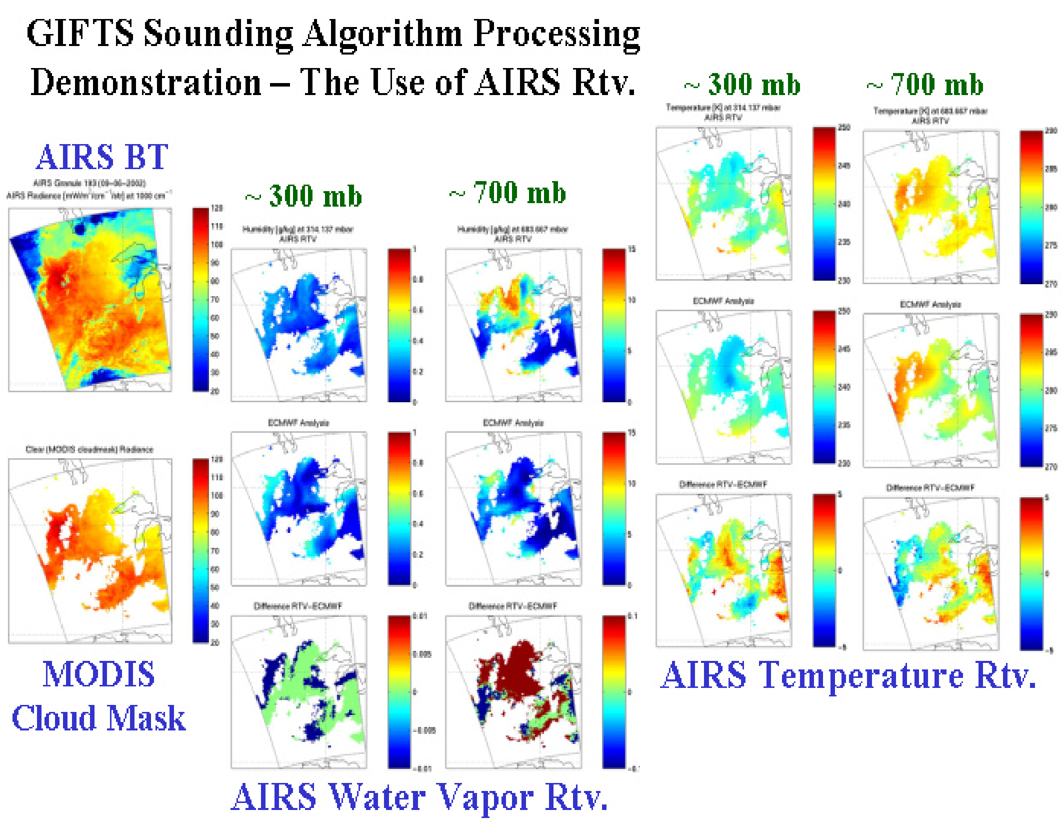

Fig. 11: GIFTS retrieval processing as demonstrated using EOS Aqua AIRS temperature and water vapor retrievals where cloudy fields of view identified by the MODIS cloud mask have no data.

5. HYPERSPECTRAL ALTITUDE- RESOLVED WATER VAPOR TRACKED WIND

By tracking altitude-resolved water vapor fields provided by GIFTS retrievals available from multiple time steps wind profiles of high vertical resolution can be achieved.

Figures 13, 14, and 15 present the current progress of altitude-resolved water vapor tracking to produce improved wind vectors that no longer contain the ambiguity of height assignment suffered by traditional radiance tracking. Three different types of water vapor tracers coupled with tracking algorithm refinement are used with both simulated and airborne hyperspectral retrievals to assess the performance of this new geosynchronous retrieval derived wind concept.

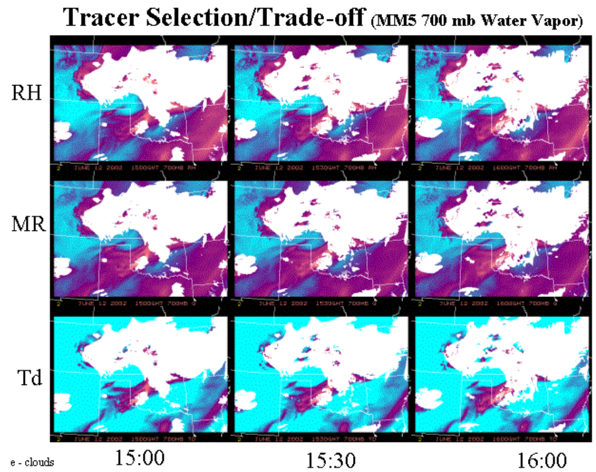

Fig. 13: Three different water vapor tracers: relative humidity (RH), mixing ratio (MR), and dew point (Td) derived for a trade-off study of water vapor tracked winds.

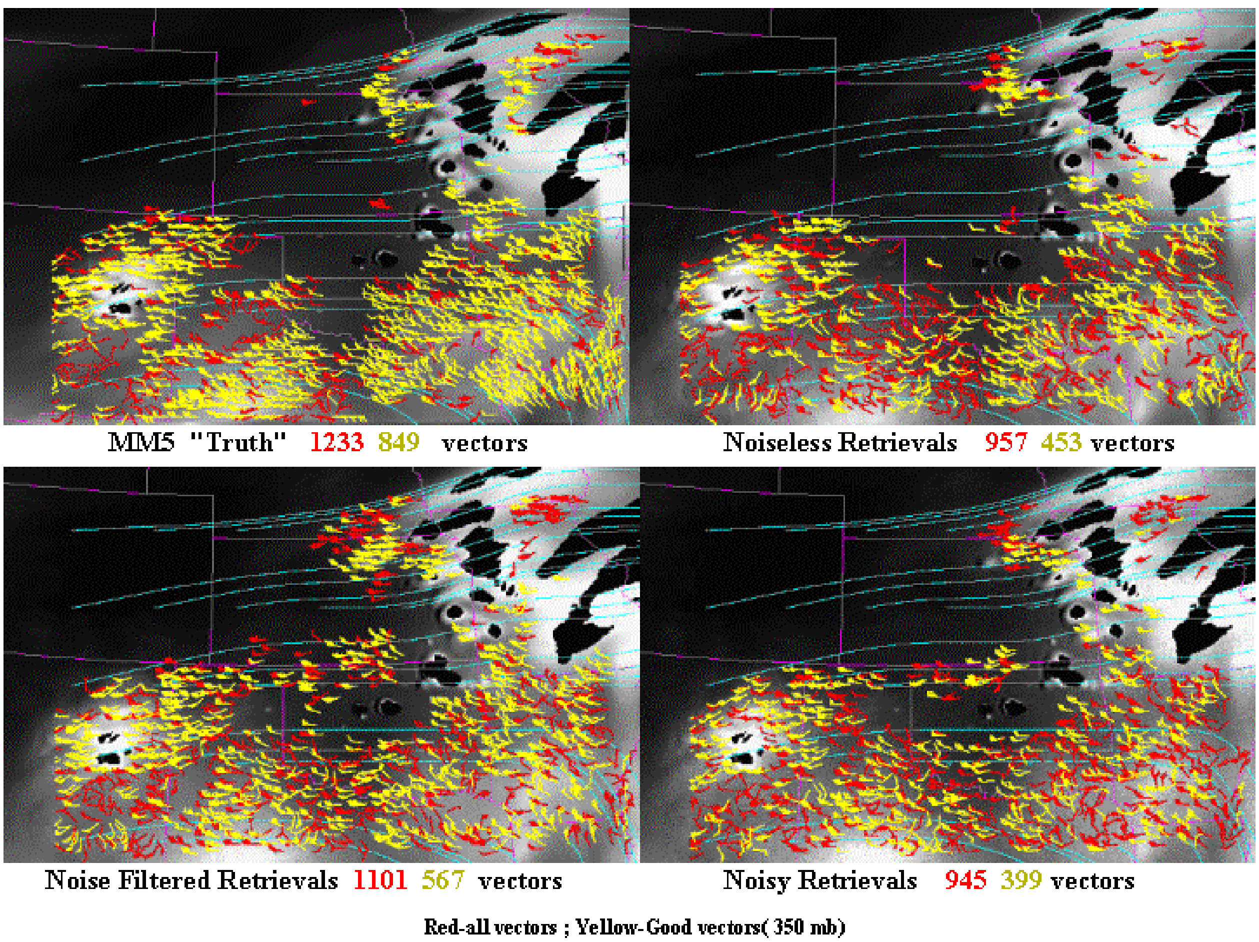

Fig. 14: Trade-off analysis of 350 mb water vapor retrieval tracked wind analysis. Four experiments using water vapor of MM5 model (as “truth”, upper left), noiseless GIFTS retrieval (upper right), noise filtered GIFTS retrieval (lower left), and nominal noisy GIFTS retrieval (lower right) are shown. Yellow vectors are acceptable while red vectors are not by quality control.

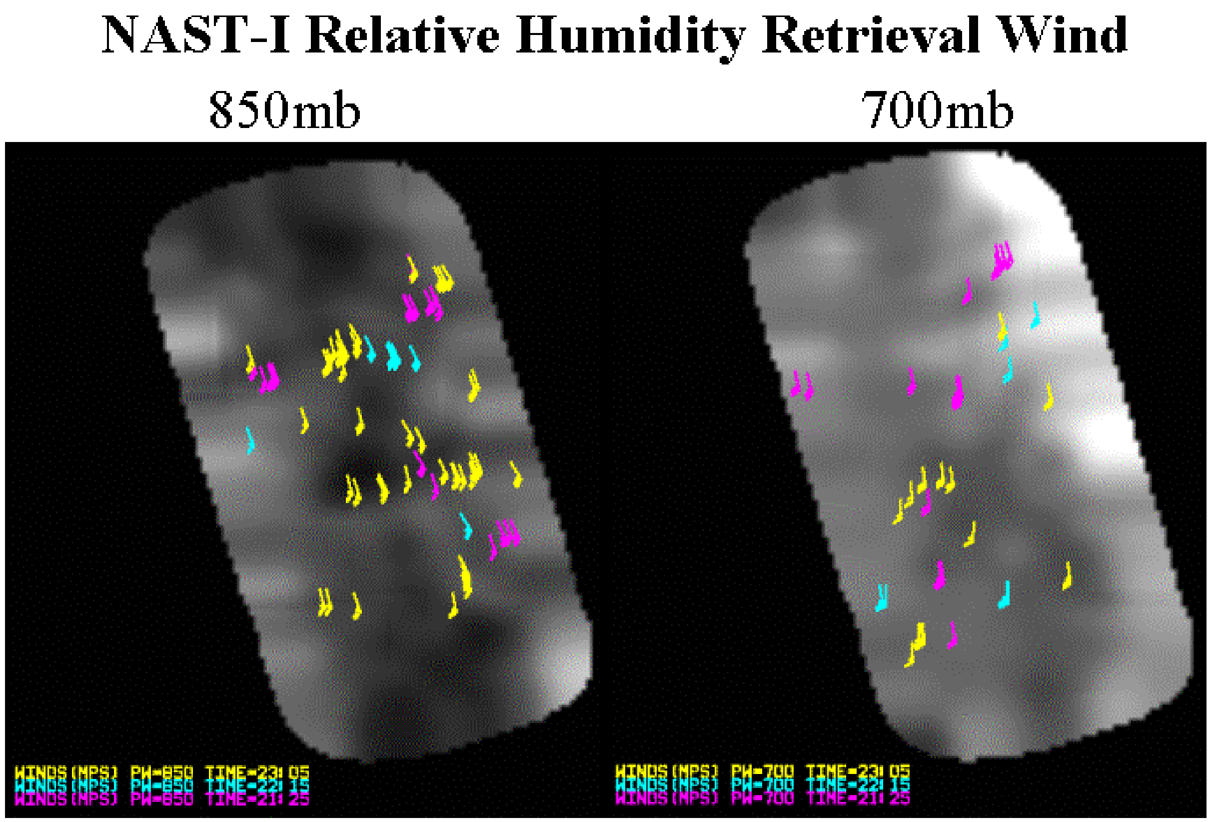

Fig. 15: Wind vectors derived from the tracking of NAST-I water vapor profile retrieval of 700 and 850 mb, respectively. Vectors with magenta, cyan, and yellow colors are for 21:25, 22:15, and 23:05 UTC, respectively.

6. SUMMARY

In this manuscript, progress is reported in conducting GIFTS measurement simulations for spatially and spectrally coherent clear, cloudy, land (IHOP) and oceanic – (THORPEX) scenes that originate from mesoscale modeling of the atmosphere. With the ongoing modeling of gases and cloud absorption and emission, and parameterized fast cloud radiative transfer calculation, high temporal resolution animation of water vapor and spectral images can provide an early insight into GIFTS sounding and water vapor tracked wind capability. Using a linear Principal Component Regression retrieval and water vapor tracking approaches, sensor sounding profile and water vapor altitude resolved wind vector performance are analyzed. The GIFTS project, under the joint support of NASA/Navy/NOAA, will continue to evolve. NASA will validate the technology and measurement concept aspect of the program; the Navy will continue to support basic research to advance broad use of GIFTS measurements over an oceanic target area; and NOAA will develop ground processing capability to validate operational measurement and product usage for risk reduction of any future geostationary advanced hyperspectral sounders.

ACKNOWLEDGEMENT

This research is jointly supported by Navy MURI grant N00014-01-1-0850, NOAA GIFTS PAP grant NA07EC0676, and NASA GIFTS NAS1-00072.

REFERENCES

Clough, S. A., and M. J. Iacono, 1995: Line-by-line calculations of atmospheric fluxes and cooling rates. 2: Applications to carbon dioxide, ozone, methane, nitrous oxide and the halocarbons. *J. Geophys. Res.*, **100**, 16519–16535.

Grell, G. A., J. Dudhia and D. R. Stauffer, 1994: A description of the fifth-generation Penn State/NCAR mesoscale model (MM5), *NCAR Tech. Note TN-398+STR*,117 pp.

Hannon, S., L. L. Strow, and W. W. McMillan, 1996: Atmospheric infrared fast transmittance models: A comparison of two approaches, in Proceedings of SPIE Conference 2830, Optical Spectroscopic Techniques and Instrumentation for Atmospheric and Space Research II (12pp.).

Huang, H.-L., H. E. Revercomb, J. Thom, P. B. Antonelli, B. Osborne, D. Tobin, R. Knuteson, R. Garcia, S. Dutcher, J. Li, and W. L. Smith, 2000: Geostationary Imaging FTS (GIFTS) Data Processing: Measurement Simulation and Compression. Proceedings of SPIE, William L. Smith and Yoshifumi Yasuoka, editors. *Hyperspectral Remote Sensing of the Land and Atmosphere*. 9-12 Oct. 2000, 103-114.

Mlawer et al., 2003: A New Water Vapor Continuum Model: MT_CKD_1.0, Thirteenth ARM Science Team Meeting, Broomfield, CO, 31 March - 4 April 2003.

Rothman, L. S., R. R. Gamache, R. H. Tipping, C. P. Rinsland, M. A. H. Smith, D. C. Benner, V. Molathy Devi, J.-M. Flaud, C. Camy-Peyret, A. Perrin, A. Goldman, S. Massie, L. R. Brown, and R. A. Toth, 1992: The HITRAN Molecular Database: Editions of 1991 and 1992, *Journal of Quantitative Spectroscopy and Radiative Transfer*, 48, 469–507.

Smith, W. L., D. K. Zhou, F. W. Harrison, H. E. Revercomb, A. M. Larar, H.-L. Huang, and B. Huang, 2000: Hyperspectral remote sensing of atmospheric profiles from satellites and aircraft, Proceedings of SPIE, William L. Smith and Yoshifumi Yasuoka, editors. *Hyperspectral Remote Sensing of the Land and Atmosphere*. 9-12 Oct. 2000, 94-102.

Stamnes, K., S-C., Tsay, W. Wiscombe, K. Jayaweera, 1988: Numerically stable algorithm for discrete-ordinate method radiative transfer in multiple scattering and emitting layered media". *Appl. Opt.*, 27, 2502–2509.

Turner, D., 2003: Microphysical properties of single and mixed-phase Arctic clouds derived from ground-based AERI observations. Ph.D. thesis. University of Wisconsin - Madison, Madison, Wisconsin.

Yang, P, B-C Gao, B.A. Baum, Y. X. Hu, W. J. Wiscombe, S.-C. Tsay, D. M. Winker, S. L. Nasiri, 2001: Radiative properties of cirrus clouds in the infrared (8-13 μm) spectral region. *Journal of Quantitative Spectroscopy and Radiative Transfer*, **70**, 473-504.

Yang P, Liou K. N., 1996: “Finite-difference time domain method for light scattering by small ice crystals in three-dimensional space”. *J Opt. Soc. Amer. A*; **13**, 2072-2085.